NANO LETTERS

2005
Vol. 5, No. 7
1351−1356

Optically Fabricated Three Dimensional Nanofluidic Mixers for Microfluidic Devices

Seokwoo Jeon,[†,||,⊥] Viktor Malyarchuk,[†,⊥] Jeffrey O. White,[⊥] and John A. Rogers*[,†,‡,§,||,⊥]

Department of Materials Science and Engineering, Department of Electrical and Computer Engineering, Department of Chemistry, Beckman Institute, and Frederick Seitz Materials Research Laboratory, University of Illinois at Urbana/Champaign, Urbana, Illinois

Received March 30, 2005; Revised Manuscript Received May 11, 2005

ABSTRACT

This paper describes a simple technique for fabricating complex, but well defined, three-dimensional (3D) networks of nanoscale flow paths in the channels of microfluidic systems. Near field scanning optical measurements reveal the optics associated with the fabrication process and the key features that enable its application to the area of microfluidics. Confocal studies of microfluidic devices that incorporate 3D nanostructures formed using this approach show that they function as efficient passive mixing elements, particularly at low Reynolds numbers. This application and others such as separation and extraction in microfluidic total analysis systems or lab on a chip devices represent promising areas for 3D nanostructures of this general type.

Devices that perform controlled mixing are critical components of microfluidic total analysis systems (μ-TAS). Without such devices, flow in μ-TAS is simple, uniaxial laminar, due to low Reynolds numbers, $\mathrm{Re} = Vl/v$, where V is flow velocity, l is channel dimension, and v is fluid viscosity. Mixing proceeds only by diffusion and requires unacceptably long path lengths: from several to many millimeters for moderate flow rates (∼0.25−1 mm/s) in 200 μm channels.[1,2] Active or passive mixers can generate transverse components of flow to induce mixing over relatively short distances.[3,4] Active devices based on rotating magnetic microstir bars,[5] acoustic cavitation cells,[6] pneumatically pumped rings,[7] and others have excellent performance and can be small in size.[4] The complexity of these components and the need to supply power to them make their integration into μ-TAS challenging. Passive devices, on the other hand, achieve mixing simply through the use of channels with clever designs.[1−3,8−11] These mixers are relatively easy to integrate, but most have efficiencies that are low compared to those of active systems. Tesla[2] and three-dimensional (3D) serpentine[12] passive mixers have high efficiencies, but they require long (∼1 cm) path lengths and they work best at high Re (> 5) for channel dimensions ∼100−200 μm. Chaotic passive mixers[9] that use relief structures in the channels operate efficiently over a wide range of Re numbers, even at very high Péclet number, but they also require long (∼3 cm) path lengths. Other devices create multiple (2−30) substream flows that weave through each other. These mixers can be compact (0.3−3 mm in length)[2,3,8] but they can be difficult to implement with small channel dimensions since the structures that generate the substream flows demand patterning with resolution that is substantially higher than that needed for the channels.

This paper describes a type of substreaming device in which large numbers (>2000) of lithographically defined 3D nanofluidic pathways (50−300 nm wide) completely fill the cross section of a microfluidic channel. These 3D structures enhance mixing even at small Re (<1), where chaotic advection is unlikely to be signficant.[13] Conceptually similar systems that use random nanoporous polymers and colloidal spheres have been investigated recently.[1,14] The approach introduced here achieves high performance with 3D polymeric nanostructures that have well defined designs and are formed directly in the microchannels using an optical technique referred to as proximity field nanopatterning.[15,16] The paper begins by describing this technique and near field characterization of the optics associated with it. Strategies for using this method to generate passive mixers in microfluidic channels are then presented. Cross sectional confocal microscopy analysis indicates efficient operation at flow rates

* Corresponding author: E-mail: jrogers@uiuc.edu.
† Department of Materials Science and Engineering.
‡ Department of Electrical and Computer Engineering.
§ Department of Chemistry.
|| Beckman Institute.
⊥ Frederick Seitz Materials Research Laboratory.

10.1021/nl050606r CCC: $30.25
Published on Web 05/28/2005

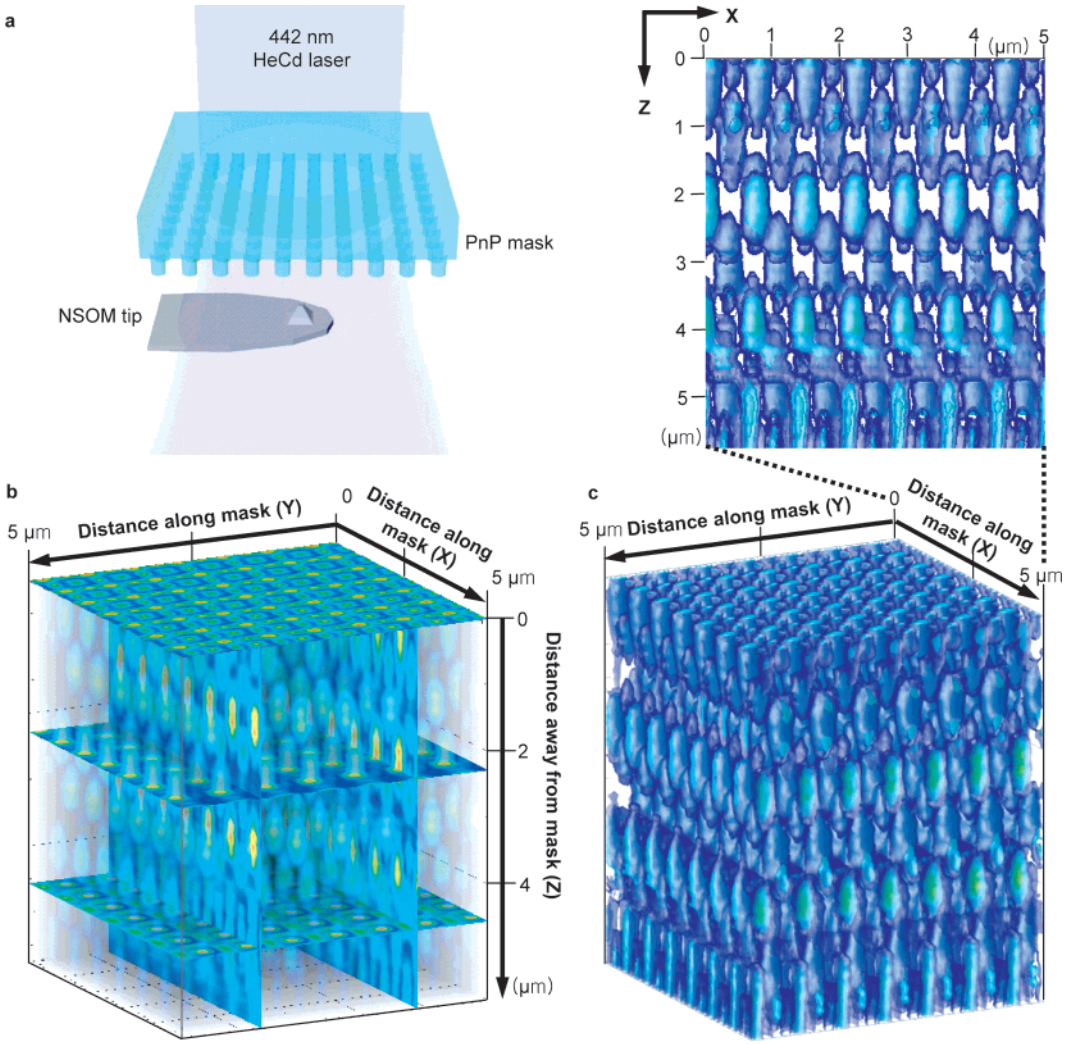

Figure 1. (a) Schematic illustration of the experimental setup for near field scanning optical microscopy (NSOM) of intensity distributions formed by passage of light (442 nm HeCd laser) through a phase mask that consists of a square array of cylindrical holes with 570 and 420 nm diameters and heights, respectively, spaced by 710 nm. (b) Three-dimensional (3D) plot of the measured intensity distribution. (c) Solid form 3D plot of the intensity distribution after applying of a cutoff filter that approximates the photopolymer exposure and development process. The nanostructured mixers described here have geometries similar to that shown in (c). The spaces between the interdigitated pillars form nanoscale (50−350 nm) paths for fluid flow.

up to 10 mm/s in 25 × 100 μm microchannels, even with devices that occupy small areas (~1 mm^2). This level of performance, together with the ease of fabricating such mixers with deterministic control over their geometries, suggests that this form of passive mixing might be valuable for μ-TAS and lab-on-a-chip applications.

Proximity field nanopatterning (PnP)[15,16] is a type of photolithographic technique that uses a transparent, conformable phase mask with sub-wavelength features of relief embossed onto its surface. This relief modulates the phase of light transmitted through the mask to generate a complex distribution of intensity near its surface. We used near field scanning optical microscopy (NSOM) to evaluate directly this intensity distribution. Figure 1a illustrates the experimental geometry. Measurements used an AlphaSNOM instrument from WITec Instruments Corp. with a HeCd laser operating at 442 nm. The mask consists of a structure of polyurethane (NOA 73, Norland Products Inc.) formed by replica molding against a ~1 cm thick piece of poly(dimethylsiloxane) (PDMS) with a square array of posts embossed on its surface (570 nm diameter with 420 nm height, spaced 710 nm, fabricated by casting and curing against a pattern of photoresist on a silicon wafer).

The fabrication process described below relies on PDMS elements as the phase masks. NSOM measurements directly with PDMS masks are difficult, due to the tendency of the atomic force microscope type NSOM tip to stick to the low modulus surface of the PDMS. Figure 1b shows a 3D rendering of the intensity as a function of position along and away from the surface of the mask. The periodic variation in intensity with distance from the mask is related to the well-known self-imaging, or Talbot, effect. Exposing a photopolymer placed at the surface of the mask and then developing away the unexposed regions can produce a solid form replica in the geometry of the intensity pattern. Figure 1c shows a 3D plot generated by applying a sharp cutoff filter to the data of Figure 1b in a manner that simulates, in a simple way, the exposure and development steps.

The polymer structures used in this paper have overall geometries similar to that of Figure 1c, but with substantially smaller structural features, due to the ultraviolet (UV) exposure wavelengths and the higher refractive index of the photopolymer than air. The minimum feature size is determined, ultimately, by the optics. Well-controlled variations in intensity that have length scales as small as one-quarter of the exposure wavelength can be produced with masks of this type. NSOM measurements show that, with suitable illumination conditions, there is no loss of resolution with distance away from the mask surface, even for intensity features with sub-wavelength dimensions, up to the limits of translation of the stages used for our microscope (~25 μm). Scanning electron micrographs of structures formed using these intensity distributions, according to procedures described in the following, show effective working distances of > 200 μm.

All of the optics for PnP are built into the conformable mask. A critical feature of this element is that it can spontaneously form atomic scale, conformal "wetting" contacts with flat surfaces. This wetting process, which is driven by generalized adhesion forces,[17] generates precise optical alignment (angle and position) in the direction perpendicular to surface of the mask. Placing such a mask into contact with a thick layer of a transparent photopolymer, passing UV light through the mask, removing the mask, and then developing the photopolymer generates a solid three-dimensional replica of the distribution of intensity near the mask. The structures have geometries defined by the exposure wavelength and the layout of the mask. The mixing structures that we tested in a flow channel have shapes that are similar to that shown in Figure 1c. Features of this technique that make it well suited to applications in microfluidics include (i) capability to pattern substream flow paths with dimensions down to 50−100 nm, thereby making it suitable for use in microfluidic systems that have channel dimensions as small as a few microns, (ii) compatibility with mechanically robust photopolymers that can be easily integrated into microfluidic systems, (iii) long depth of focus and working distance to allow patterning of nanostructures throughout the depth of a microfluidic channel, and (iv) operation that requires only simple apparatus (i.e., the procedure can be carried out with a handheld ultraviolet lamp).

Figure 2 illustrates the steps for building a microfluidic device with a built-in 3D nanofluidic passive mixer. First, a thick (25 μm) uniform layer of a transparent photopolymer (SU-8) was spin cast onto a clean glass slide using a two-layer scheme to promote adhesion between glass and SU-8.[16] Exposing the SU-8 to UV light (KarlSuss MJB3 mask aligner) through an amplitude mask with transparent regions in the geometry of a Y-junction microfluidic channel defined the layout of the overall system. A short postbake (95 °C for 3 min on hotplate) formed a 25 μm thick cross-linked SU-8 structure (Figure 2a) in this Y-junction geometry. A second UV exposure (355 nm output of a frequency tripled Nd:YAG laser; Uniphase) through an amplitude mask with a 1000 μm wide transparent slit on top of a thin PnP phase

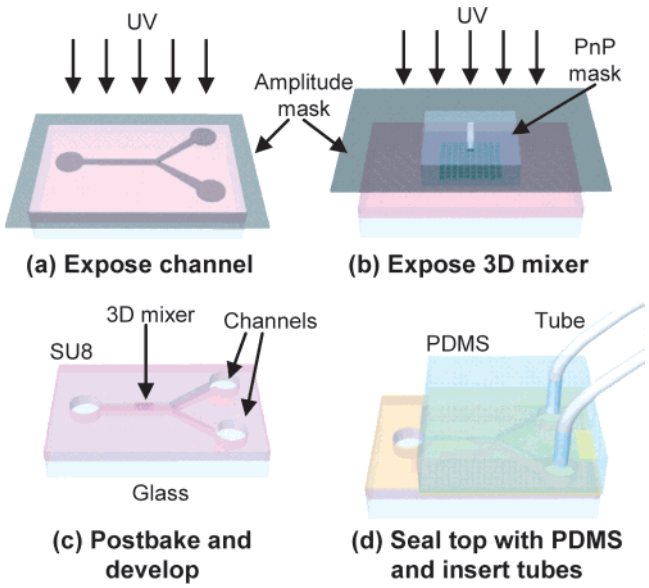

Figure 2. Schematic illustration of steps for (a) defining a Y-junction microchannel structure with an amplitude mask and for (b) defining an integrated 3D periodic nanostructure using a conformable phase mask backed with an amplitude mask. (c) Developing away unexposed regions of the polymer yields a 3D nanostructured mixer integrated with a simple microfluidic system. (d) Sealing the top with PDMS through cold welding and introducing fluid flow lines complete the device.

mask defined the 3D nanostructure. The relief on the PnP mask consisted of a square array of cylindrical posts with 375 and 420 nm diameters and heights, respectively, spaced by ~570 nm. The distribution of intensity generated by passing 355 nm light through this element has an overall geometry that is similar (but not identical) to that shown in Figure 1. Postbaking (70~75 °C for 5 min in an oven) the sample, developing it (SU-8 developer, Microchem Corp.), transferring it directly to ethanol, and then drying it in air produced a Y-junction microfluidic channel with an integrated 3D nanofluidic mixer. The use of ethanol for the drying step reduces damage that can occur to the 3D structure when capillary forces associated with drying act on the SU-8 while it is saturated and swelled by the developer. Bonding a flat piece of PDMS to the SU-8 structure by cold welding[18] between uniform layers of Ti/Au (2/5 nm by electron beam evaporation) deposited on top of the PDMS and SU-8 formed a sealed microfluidic system. Machining holes through the PDMS and inserting tube connections completed the device.

Figure 3a shows an image of a typical device. Mixers with three different geometries were used: a 90° serpentine channel, 2100 μm long (mixer 1, Figure 3a−f); a 60° serpentine channel, 1500 μm long (mixer 2, Figure 3g); a straight channel, 1000 μm long (mixer 3, Figure 3h). We also created, as a control, a device with a 90° serpentine channel, 2100 μm long, but without a mixer (no mixer). All of the mixers have the structure illustrated in Figure 3d, e, and f. (Figure 3f was collected from a sample exposed in the same manner but not integrated into a microfluidic channel). The 3D structure fills the channels and consists of periodically spaced pillars with diameters of ~300 nm and separations of ~570 nm and smaller (> 50 nm) secondary

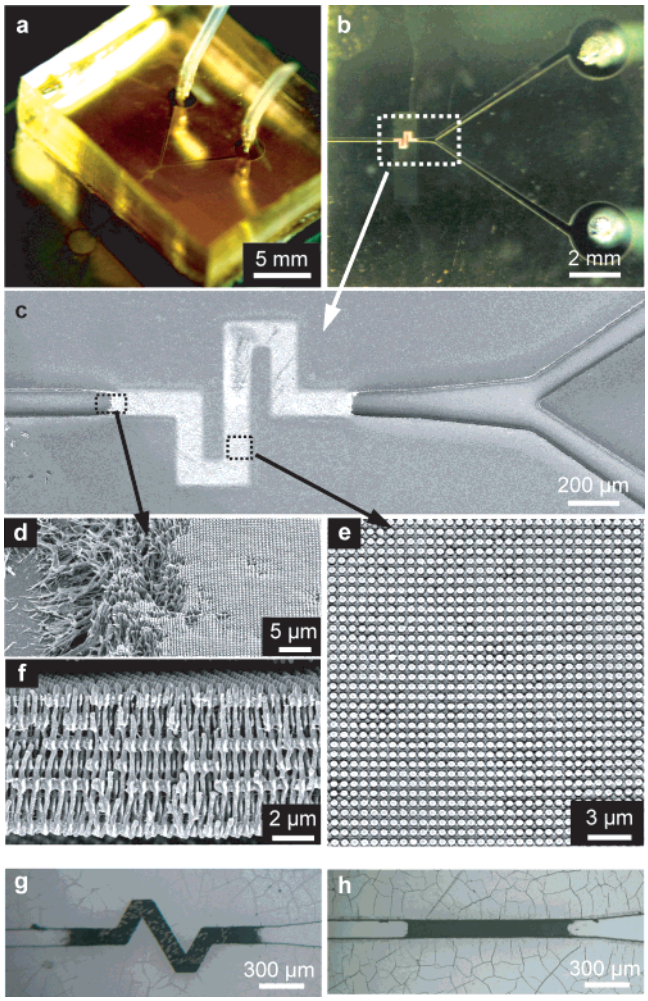

Figure 3. Optical micrograph of an assembled mixer 1 (a) and a magnified image showing the 3D nanostructure (b). Scanning electron micrograph (SEM) of a 3D mixer embedded in a serpentine microfluidic channel (c). SEM of 3D structures at the outlet (d) and in the middle (e) of the mixer. (f) Cross-sectional view of a 3D structure similar to the ones used in the mixers. The channels that exist in these systems have dimensions between 50 and 300 nm. The fabrication used conformable phase masks with relief structures in the form of a square array of 420 nm high circular dots (diameter: 375 nm, duty cycle: 35%). Optical microscope images of mixer 2 (g) and mixer 3 (h).

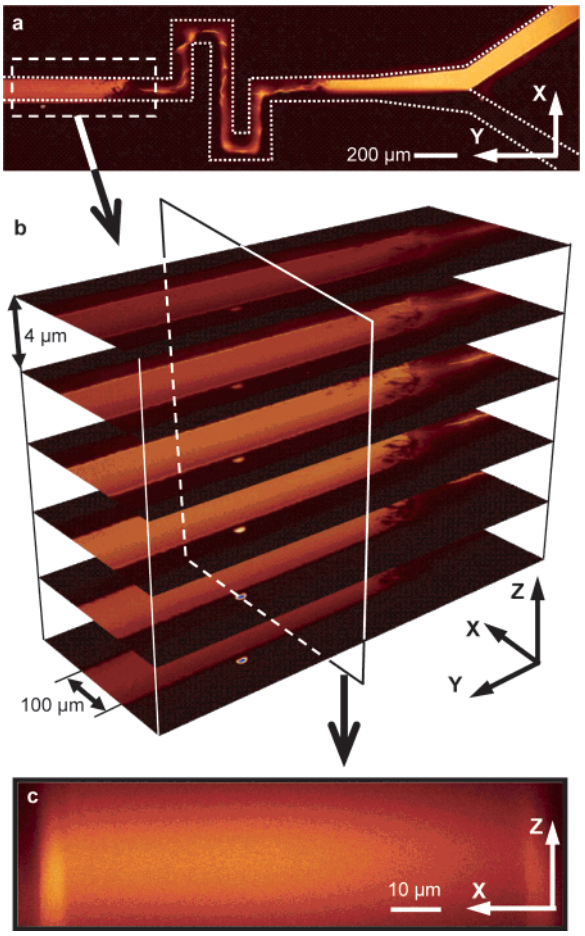

Figure 4. Confocal microscopy images of mixer 1 at a flow velocity of 6.67 mm/s. The red in these images corresponds to fluorescence recorded from Rhodamine dye in water using Ar-ion laser excitation at 514 nm. (a) Top view reveals the mixing of two fluids consisting of Rhodamine in water (top) and pure water (bottom), after passing through nanofluidic mixer 1. Series of confocal images collected at the outlet of the mixer at various distances through the thickness of the channel (steps of 4 microns) (b) and a cross-section image (c).

structures. Approximately 17 interdigitated layers of these pillars fill the channel along 25 μm thickness. Nanoscale pathways (50−300 nm wide) for fluid flow exist between these pillars. Heterogeneities (i.e., defects) in the structures can also influence the overall flow pathways.

Figure 4a shows two streams pumped through the system at velocities of 6.67 mm/s with a dual syringe pump (Stoelting Co.). The top stream consists of a low concentration aqueous solution of the fluorescent dye Rhodamine 6G (10^{-4} M). The bottom stream is pure distilled water. The flows did not appear to disrupt, to any noticeable extent, the polymeric 3D structures during the 5−10 h operation and range of flow velocities (0.01 to 50 mm/s) used for the experiments. The devices did show structural damage at very high flow velocity (~100 mm/s), but failures in these cases were usually due to breaking of the seal between SU-8 and flat PDMS. A series of confocal fluorescent microscope images at different depths (Figure 4b) and a cross-sectional view (Figure 4c) at the outlet of mixer illustrate the level of mixing that can be achieved. (We note that it was not possible to perform cross-sectional confocal measurements in the areas of the mixers, due to the large degree of scattering produced by the 3D structures.) Although the details of the operation of these complex structures are difficult to define completely, we believe that an important aspect is based on the concept of "lamination", as illustrated in Figure 5. In particular, the interdigitated 3D structures in the mixers can split flows vertically, thereby enabling them to move transversely relative to one another. Recombination of these flows after this transverse motion constitutes a lamination process that reduces the characteristic time, $\tau \sim l^2/D$, where l is stream separation, D is diffusivity, needed to achieve diffusive mixing. Other mechanisms, such as transverse flows induced in a given plane by passage through the pillars, especially in the presence of the heterogeneity in the 3D structures, may also be important. Chaotic advection and

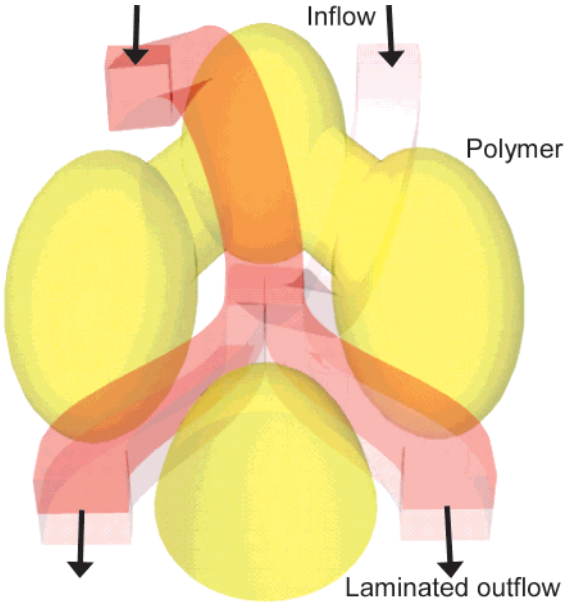

Figure 5. Schematic illustration of vertical lamination of flow streams that pass through a three-dimensional unit cell similar to that of the mixers described here. This lamination mechanism reduces the distance (and, therefore, the time) over which diffusion must occur to achieve mixing.

recirculating eddies may also contribute to mixing, but they are unlikely to be significant for the range of flow rates and channel geometries investigated here, partly due to the extremely low Re associated with flows through the nanochannels.[2] In a straight, open channel without a mixer, the fluids require a path length ($\sim\tau V$) of ~70 mm to be mixed.

To investigate further the characteristics of these mixers, we compared the efficiencies of mixer 1−3 and no mixer at different flow rates. To quantify the efficiencies, we collected cross-sectional confocal images of the channels just after the end of the mixers and subtracted their background intensities (as evaluated from dark regions located far away from the channels). We then computed integrated intensities up to, but not including, the regions directly adjacent to the channel walls. (This procedure uses approximately 90% of the width and height of the cross-section. The rectangles indicated in dashed lines in the upper frame of Figure 6d indicate the areas that were used.) The integrated intensities evaluated from the halves of the channels just after the mixers (the right halves indicated in the inset images of Figure 6d) were divided by the integrated intensities evaluated across the entire channel. For the no mixer case, instead of cross-sectional images, we used, for convenience, in-plane confocal images collected along a 500 μm length of the channel at the midpoint in its depth. This procedure is equivalent to the cross-sectional approach, since the fluid distribution in the no mixer case does not vary with channel depth. With either procedure, 0.5 corresponds to complete mixing; <0.5 corresponds to incomplete mixing. Both of these simple methods for quantifying the degree of mixing are suitable for our systems and lead to smooth, gradual intensity variations without the type of fine structures observed at the outputs of other classes of mixers. Efficiencies are comparable for all mixers at the lowest flow rate. Here, purely

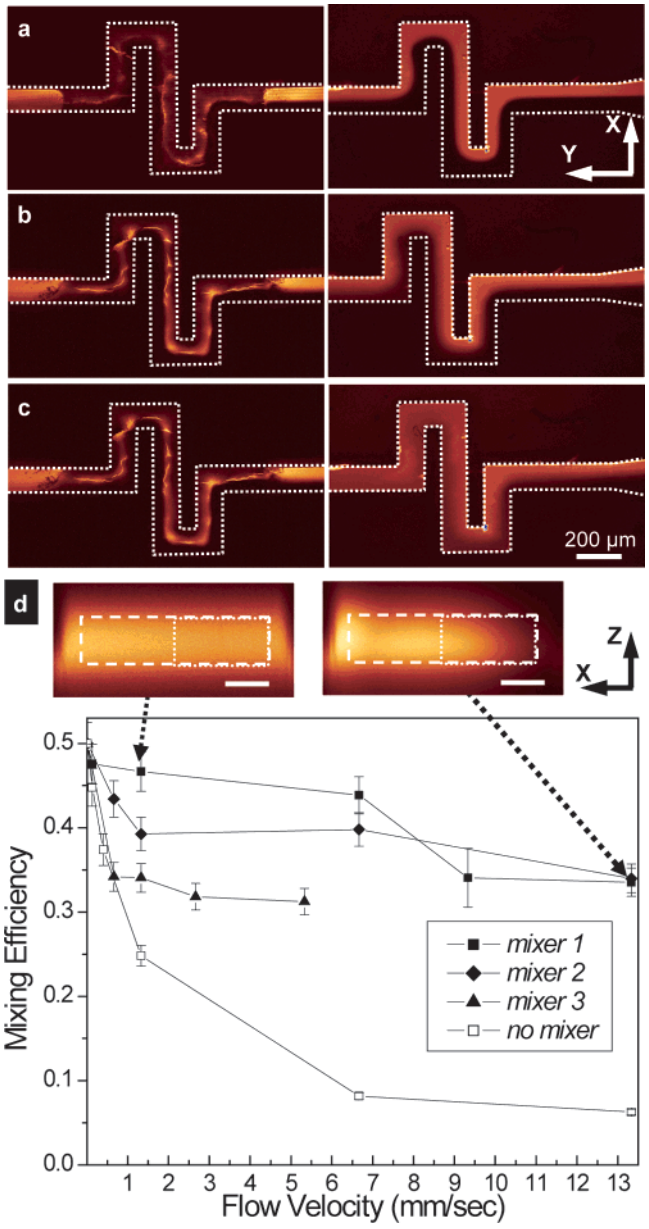

Figure 6. Confocal microscopy images of mixer 1 (left frames) and no mixer (right frames) showing different levels of mixing at flow velocities of 13.3 mm/s (a), 1.33 mm/s (b), and 0.133 mm/s (c). (d) Mixing efficiency as a function of flow velocity with four different mixers. Cross section of mixer 1 at 1.33 mm/s (inset left) and 13.3 mm/s (inset right), scale of inset images: 25 μm. The white dashed squares in the insets illustrate the areas of the channel cross sections that were used to compute the mixing efficiencies.

diffusive mixing, even without any 3D structure (i.e., no mixer), is possible because the times for passage through the channels are longer than l^2/D (~10 s). As the flow rate increases, the efficiency of no mixer drops rapidly, while those of mixers 1−3 drop much more slowly. In this regime, the 3D structures are important to facilitate mixing. The performance is significantly better than that of random nanoporous mixers,[1] which require 10 mm channel lengths to mix at flow velocities of 1 mm/s at similar Re and with similar channel dimensions. The decrease in efficiencies of mixers 1−3 with increasing flow rate is consistent with a mixing mechanism that does not depend strongly on turbulent

flow or chaotic advection, both of which would be expected to increase sharply with flow rate. The geometries that involve bends in the regions with the 3D structures (i.e., mixers 1 and 2) tend to have higher efficiencies than those that incorporate only straight channels (i.e., mixer 3). The different path lengths through the 3D structures in mixers 1−3 partially account for these differences in efficiency. To remove, approximately, the effects of different lengths, the flow velocities can be scaled linearly by the lengths. (This type of scaling is strictly valid only under the condition of purely diffusive mixing.) After this type of scaling, it is still the case that the mixing efficiencies increase with the number of bends. It is possible that the bends promote mixing by redirecting flow at these locations (i.e., the nodes), in a manner similar to the operation of serpentine mixers without 3D structures.[12]

In conclusion, compact devices that use 3D nanostructures generated by PnP can serve as passive mixers with high performance, especially at relatively low Re, where enhanced mixing by chaotic advection is difficult. A drawback of these mixers is that they can be susceptible to clogging, due to the very small dimensions of the flow paths, and they can create significant pressure drops. On the other hand, the very small characteristic sizes of the 3D flows within the mixers enables them to be scaled for use in microfluidic systems with channel geometries that are much smaller than those illustrated here. In addition, the small flow paths, taken together with the associated high surface area-to-volume ratios and the ease of fabrication, suggest additional possible uses in capillary electrophoresis, high-pressure liquid chromatography and other microfluidic devices.

Acknowledgment. Part of this work was carried out in the Laser and Spectroscopy Facility of the Frederick Seitz Materials Research Laboratory, University of Illinois, which is partially supported by the U.S. Department of Energy under grant DEFG02-91-ER45439. This work was also funded by partial support from National Science Foundation under grant DMII 03-55532, the center for Nanoscale Chemical Electrical Mechanical Manufacturing Systems in University of Illinois, which is funded by National Science Foundation under grant DMII-0328162. S.J. thanks the Beckman Foundation for a graduate fellowship. We thank Dr. R. Cirelli and the New Jersey Nanotechnology Center for the projection mode photolithographic "masters" used to build the conformable masks described here.

References

(1) Rohr, T.; Yu, C.; Davey, M. H.; Svec, F.; Frechet, J. M. J. *Electrophoresis* **2001**, *22*, 3959−3967.
(2) He, B.; Burke, B. J.; Zhang, X.; Zhang, R.; Regnier, F. E. *Anal. Chem.* **2001**, *73*, 1942−1947.
(3) Kakuta, M.; Bessoth, F. G.; Manz, A. *Chem. Rec.* **2001**, *1*, 395−405.
(4) Campbell, C. J.; Grzybowski, B. A. *Philos. Trans. R. Soc. London A* **2004**, *362*, 1069−1086.
(5) Lu, L.-H.; Ryu, K. S.; Liu, C. *J. MEMS* **2002**, *11*, 462−469.
(6) Liu, R. H.; Lenigk, R.; Druyor-Sanchez, R. L.; Yang, J.; Grodzinski, P. *Anal. Chem.* **2003**, *75*, 1911−1917.
(7) Thorsen, T.; Maerkl, S. J.; Quake, S. R. *Science* **2002**, *298*, 580−584.
(8) Kenis, P. J. A.; Ismagilov, R. F.; Whitesides, G. M. *Science* **1999**, *285*, 83−85.
(9) Stroock, A. D.; Dertinger, S. K. W.; Ajdari, A.; Mezit, I.; Stone, H. A.; Whitesides, G. M. *Science* **2002**, *295*, 647−651.
(10) Hong, C.-C.; Choi, J.-W.; Ahn, C. H. *Lab on a Chip* **2004**, *4*, 109−113.
(11) Neils, C.; Tyree, Z.; Finlayson, B.; Folch, A. *Lab on a Chip* **2004**, *4*, 342−350.
(12) Liu, R. H.; Stremler, M. A.; Sharp, K. V.; Olsen, M. G.; Santiago, J. G.; Adrian, R. J.; Aref, H.; Beebe, D. J. *J. MEMS* **2000**, *9*, 190−197.
(13) Branebjerg, J.; Gravesen, P.; Krog, J. P.; Nielson, C. R. In *Proc. IEEE MEMS Workshop*: San Diego, CA, 1996; pp 441−446.
(14) Seong, G. H.; Crooks, R. M. *J. Am. Chem. Soc.* **2002**, *124*, 13360−13361.
(15) Jeon, S.; Menard, E.; Park, J.-U.; Maria, J.; Meitl, M.; Zaumseil, J.; Rogers, J. A. *Adv. Mater.* **2004**, *16*, 1369−1373.
(16) Jeon, S.; Park, J.-U.; Cirelli, R.; Yang, S.; Heitzman, C. E.; Braun, P. V.; Kenis, P. J. A.; Rogers, J. A. *PNAS* **2004**, *101*, 12428−12433.
(17) Hsia, K. J.; Huang, Y.; Menard, E.; Park, J. U.; Zhou, W.; Rogers, J.; Fulton, J. M. *Appl. Phys. Lett.* **2005**, *86*, 154106/1−154106/3.
(18) Ferguson, G. S.; Chaudhury, M. K.; Sigal, G. B.; Whitesides, G. M. *Science* **1991**, *253*, 776−778.

NL050606R